Anatomy changes and virtual restoration of statues

Tong Fu, Raphaëlle Chaine, Julie Digne

EUROGRAPHICS Workshop on ... (200x)
N.N. and N.N. (Editors)

Anatomy changes and virtual restoration of statues

Tong Fu, Raphaëlle Chaine, Julie Digne

Université de Lyon, UCBL, CNRS, France

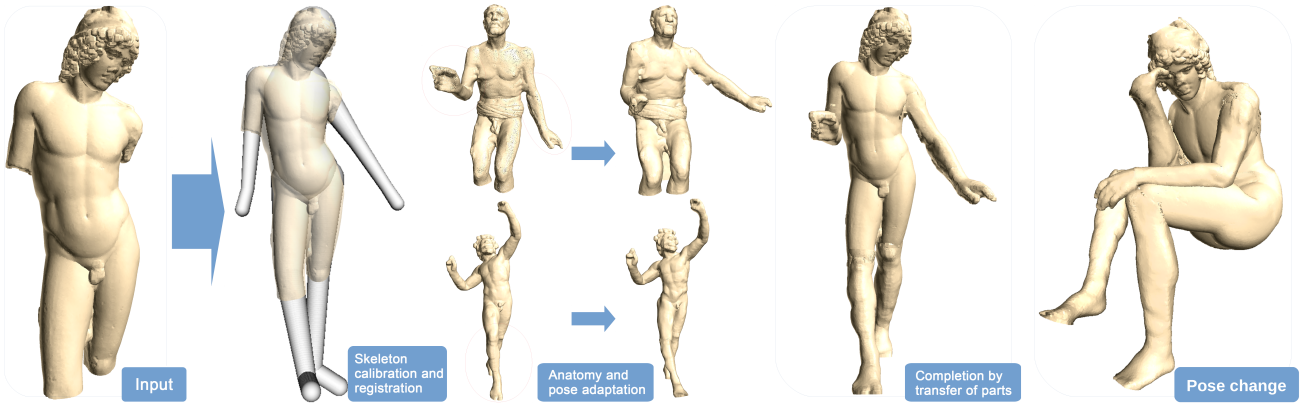

Figure 1: *Restoration and pose change of the Prince Paris statue. Through articulated model regression, we identify the anatomy and pose. We then adapt parts from other statues after a change of morphology and use them to complete the input. Once the statue is complete, we can also change its pose: here we bring it to the pose of* The Thinker *by Auguste Rodin.*

Abstract

Restoration of archaeological artefacts is an important task for cultural heritage preservation. However traditional restoration processes are difficult, costly and sometimes risky for the artefact itself, due to poor restoration choices for example. To avoid this, it is interesting to turn to virtual restoration, which allows to test restoration hypotheses, that can be later carried out on the real artefact. In this paper, we introduce a restoration framework for completing missing parts of archaeological statues, with a focus on human sculptures. Our approach proceeds by registering an anatomical model to a statue, identifying the missing parts. Compatible statues are then provided by the users and their poses are changed to match the broken statue, using a point-cloud specific skinning technique. The modified statues provide replacement parts which are blended in the original statue.

CCS Concepts

• ***Computing methodologies*** → ***Shape modeling; Point-based models;***

1. Introduction

The restoration of historical artefacts requires a comprehensive understanding of archaeology and art history. Many recommendations have been made for guiding the restoration process [ICO64]. Manual restorations being costly, invasive and sometimes even risky, museums are often reluctant to carry out such processes. On the contrary, a *virtual* restoration process gives restorers the possibility to build and test different hypotheses with minimum user intervention.

While research has mainly focused on reassembling fractured objects [ED17, HFG*06], our work focuses on the virtual restoration of incomplete human statues, provided as 3D point sets. Our idea finds its roots in the work of Grossman et al. [GPT03] who discuss varying approaches to the restoration of ancient sculptures. In particular, they discuss restoration through the combination of ancient fragments, a technique widely used in the 18th and 19th centuries. Our virtual restoration follows this idea by harmoniously combining parts belonging to different statues after bringing them to a common pose and anatomy. The process contains 3 stages.

First, we apply the FAKIR [FCD20] method to register an articulated model to the statue point set. Second, each input point is represented by its residual displacement above the registered anatomical model. This point set encoding is coupled with a skinning method to modify statue poses and proportions. All steps are achieved directly on the point cloud, avoiding thus tedious meshing steps and preserving the accuracy of initial sampling. This virtual restoration has two advantages: first, there is no limit to the number of restoration hypotheses that can be tested, second completion can be achieved using statues of different morphology and poses, avoiding thus adding an oversized arm to an undersized body. As a nod, we also illustrate that the technique of changing the pose of a statue can be used to generate new statues that could be used in the context of an animated film accompanying the description of a work in a museum. To summarize, our contributions are the following:

- A framework to realize a virtual restoration based on point set.
- A point set skinning process by using an articulated model combined with heightfield.

2. Related work

Pose and shape estimation A large body of works is dedicated to the estimation of a 3D human pose by registering a model to input data. This process is called *rigging* in animation research. Thus it is possible to register a skeleton into a mesh [BP07, TGB13]. Some works aim at pose and motion tracking from dynamic data. [SHG*11, WZC12, SBB10] register a skeleton to a depth video or a multi-view video using the silhouette information. But these approaches require a dynamic scene and cannot be applied to static data. Some human parametric mesh models [ASK*05, PMRMB15,LMR*15,HSS*09,ZB15] rely on database of human scans of various proportions and positions. The parameters are such as to best characterize the variety of existing anatomies and poses. [HLRB12,WHB11,AMX*18,JCZ19,LSS*19,MMRC20] use such models to estimate both pose and shape. But these models are not suitable for archaeological statues which can have unrealistic body proportions. The Deepcut [PIT*16] and OpenPose [CSWS17] methods tackle the pose estimation problem using Machine Learning for detecting 2D joints in images and videos. In 3D, [BKL*16] and [HBL*17] estimate the 3d human pose and shape from a single image or multi-view images by fitting a SMPL [LMR*15] model to DeepCut estimated joint positions. However CNN-Based joint detectors can only work if the nature of the data is not too different from the training data. Statues having often unrealistic human proportion and pose (See Fig. 2), these methods are doomed to fail. In contrast with learning techniques, the FAKIR algorithm [FCD20] estimates the pose and anatomy from a single point set using a simple articulated model and an inverse kinematic-based registration algorithm. Our method will rely on this algorithm that we will recall.

Pose change Once a skeleton is rigged, a skinning process can be used for pose change or animation purposes. Skinning methods aim at attaching the surface model to the skeleton by using weights that define the influence of the bones on the position of surface points. Then, when changing the pose of the skeleton, the attached surface should deform accordingly. Setting the right weights is an important question: while the profile of the weights is generally sketched by graphic designers [MTG03], there exist automatic weighting techniques that, for example, use heat diffusion [BP07, TGB13,ARM*19]. Linear Blend Skinning [MTLT88] is one of the most popular skinning approach. A mesh surface point is transformed by a linearly weighted combination of the moving bones it is attached to. This method suffers from a collapsing problem near rotating joints, which has been tackled using Pose Space Deformation [LCF00], Multi-Weight Enveloping [WP02], spherical Skinning [Kv05] and Dual Quaternions Skinning [KCvO07]. Taking a different perspective on the problem, Implicit skinning [VBG*13] uses an implicit formulation of the surface that better supports pose changes and reprojects skinned vertices on the implicit model after each pose change. In this paper, we also use a proxy model but it is explicit. A recent skinning method [LL19] corrects artefacts of Linear Blend Skinning by locally estimating the rigid transformation that best restores the relative position of a vertex with respect to its neighbors using Laplacian differential coordinates. This method, designed for meshes, involves a definition of details in terms of Laplacian differences. In our approach, we rather define the detail as the residual over the registered anatomical model. [KSH12] decomposes a movement at a joint into swing and twist to diminish the artefacts of Linear Blend Skinng and Dual Quaternions Skinning. In our work, we also decompose the bone motion into a bending motion and a twisting rotation.

When a model is rigged and skinned, it is possible to change its pose manually by interacting with some joints of the skeleton. Through the skinning weights, the mesh surface should deform accordingly. However, it is often tedious to design every single motion of each joint for each frame of an animation. As a consequence, research has focused on inferring the motion from some key joints and frames with given skeleton positions. In this inverse kinematics context, the Fabrik [AL11] and CCD [WC91] algorithms define kinematic chains and aim at transforming each chain from its input pose to its target pose by updating pose parameters one after the other alternatively forward and backward along the chain.

Shape Synthesis. Shape synthesis is often done by reusing parts of existing models [FKS*04]. The idea is to retrieve suitable models from a database and warp them to conform with an incomplete model [PMG*05,CK10]. More recently, a probabilistic representation for the components of a shape has been developed to suggest relevant components during an interactive assembly-based modeling session [CKGK11,KCKK12]. In our work, we propose a framework to statue shape synthesis by part combination, the choice of the parts being done manually while the part adaptation is automatic.

3. Method

Our goal is to replace missing parts of incomplete statues by deforming a point set of another statue. Our virtual restoration process contains three stages:

- Stage 1: Pose and anatomy estimation of statues. In this stage, we use FAKIR algorithm to register a sphere-mesh model to the target statue (the statue to be completed) and a sphere-mesh model

to each of the statues used as candidates to complete the missing parts of the target statue.
- Stage 2: Pose and anatomy changes. We use a dedicated skinning method to change the dimension and position of candidate statues by using the same dimension and pose as in the target statue.
- Stage 3: Combination. We complete missing parts of the target statue by combining the corresponding parts of candidate statues.

3.1. Stage 1: Pose and anatomy estimation using FAKIR

The analysis of artistic statues shows huge differences in proportion compared to human body. Indeed artists tend to favor the aesthetic perception over proportion realism [Hus55, New34]. Figure 2 shows an example of such unrealistic statue of the Gallo-Roman eras.

Figure 2: *An example of a statue with unrealistic anatomy: A Gallo-Roman statue of a Gallic warrior (Avignon, France, picture: F. Philibert-Caillat)*

In this context, we cannot use learning-based methods that were trained on real human data-sets and instead rely on the FAKIR registration method [FCD20] to estimate the pose and anatomy of a statue. Indeed, FAKIR has few constraints, allowing to fit a sculpture which does not comply with realistic human proportions. Below we summarize the FAKIR algorithm.

We provide FAKIR with a human body template of 22 bones $\{B_k(l_k, \mathbf{r}_k)\}_{k=1..22}$. Each bone is a truncated cone closed by two spherical caps defined by two intrinsic parameters (length l and two radii $\mathbf{r} = \{r_1, r_2\}$) and by one extrinsic parameter (vector Θ) to define the rotation with respect to its predecessor since the bones are organized into chains of consecutive bones sharing a common radius.

To measure the distance from the point set to the sphere-mesh, Fakir uses a distance function that is computed as a sum of per-bone functions. The one-bone distance function evaluates the distance between a bone and the points that are closer to that bone than to the other bones:

$$E_k = \sum_{p \in P_k} \|p - \tilde{p}_k\|^2 \tag{1}$$

In FAKIR, the quality and the speed of the minimization of all the distances are obtained by iteratively coupling one-bone distance by two, which amounts to optimizing iteratively the position of each joint in the model. Two-bone distance function thus evaluates the distance between a pair of consecutive bones and the points attached to them:

$$E_{k,k+1} = \sum_{p \in P_k} \|p - \tilde{p}_k\|^2 + \sum_{p \in P_{k+1}} \|p - \tilde{p}_{k+1}\|^2. \tag{2}$$

In both equations 1 and 2, P_k is the set of points which are closest to bone B_k, and $\tilde{p}_k$ is the projection of a point p on the bone B_k. FAKIR is a kinematic registration process which loops forward and backward through the chains of bones to rotate and re-scale bones successively. For a chain of bones, the algorithm starts by one extremity of bone B_k, keeps it fixed (roughly close to points that should correspond to it) while gradually rotating B_k around the fixed extremity and while refining the intrinsic parameters of B_k, by minimizing the one-bone distance. Then the algorithm moves to the next bone B_{k+1}, again using the one-bone distance function. After optimizing B_k and B_{k+1}, the algorithm considers them as a pair of bones and adjusts their common joint position and radius while keeping the two other extremities fixed, by minimizing the two-bone distance function. Then the next pair of bones B_{k+1} and B_{k+2} is considered and the same steps are repeated. Once a chain of bones has been positioned and scaled over its length, FAKIR repeats the process forward and backward to refine bones' parameters, this time only considering optimization of two-bones energy functions, except for the chain extremity. After several iterations, FAKIR results into a registered model representing the pose and anatomy of a statue.

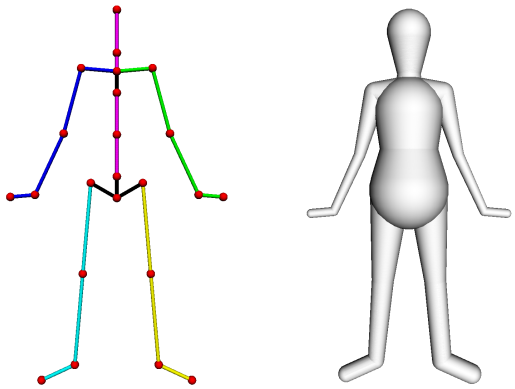

(a) *Skeleton* **(b)** *Sphere-mesh*

Figure 3: *FAKIR skeleton and sphere-mesh model. Bones are organized into 5 chains shown in different colors.*

3.2. Stage 2: Pose change by point set details skinning

Once the anatomical model is registered to the statue point set, we exploit the relative position of the points with respect to the sphere-mesh model to change the pose and the elementary anatomy of a statue by modifying the extrinsic and intrinsic parameters of the bones respectively and by reporting the point set details above it. To do so, we need to attach the detail point set to its registered articulated model so that deforming the model will deform the point set accordingly. For that purpose, we propose to associate a base-point on the articulated model to each of the original points, the originality of our approach being that those base-points may locally slide on the moving sphere-mesh to mimic the sliding of the skin on joints. For instance, some base-points can evolve from the conic section of a bone to the neighboring sphere, resulting in continuous deformation with better volume preservation than the usual linear blend skinning. In addition, special care is given to the twisting and bending rotations at each joint. The new position of the input points is then deduced from the new position of their corresponding base-points, by reporting their initial height. We will explain this heightfield skinning in section 3.2.1. For moving the base-points, we propose a new point set skinning method where the deformation at a joint is the combination of a twisting rotation and a bending rotation in section 3.2.2. Compared to existing animation approaches based on sphere-meshes, we work directly on the point set and not on a lower-resolution mesh to which a skinning algorithm can be applied after carefully setting weights. In our case the skinning is applied to the set of base-points on the sphere-mesh model with weights depending directly on the parameters of bones.

3.2.1. Heightfield skinning

Heightfield over the sphere-mesh model We propose to consider the skin of model as a set of detail-points, encoded as a set of heights on top of our articulated model, that will be transferred back on the model after pose or intrinsic parameters change. This approach is in line with displacement maps on top of polygonal models [POC05], but instead of defining a complete heightfield over the model, we define it only on base-points. The same base-point can correspond to several detail points, making it possible to handle layered details, *i.e.* folded surface sheets over the sphere-mesh model (see the Dancer with Crotales on Figure 5 and the dragon on Figure 4).

In the following, let us assume that the sphere-mesh model is registered to the point set. The heightfield value h of a point p is defined as a signed distance from p to its projection on the sphere-mesh base point $\tilde{p}$: $p = \tilde{p} + h(p)\mathbf{n}_{\tilde{p}}$, where $\mathbf{n}_{\tilde{p}}$ is the normal to the sphere-mesh surface at $\tilde{p}$ and $\tilde{p}$ is the orthogonal projection on the bone p is assigned to. Hence the surface point set is decomposed into the set of base-points on the sphere-mesh and a residual orthogonal heightfield.

Using that decomposition, any skinning algorithm can be transformed into a heightfield skinning algorithm above a sphere-mesh. The base-points are skinned using the given algorithm and then the heightfield is added back to the modified base-points yielding the final point set (Algorithm 1). It is preferential to use a skinning algorithm where base-points remain on the sphere-mesh, otherwise we re-project them on the sphere-mesh, similarly to what is done with implicit skinning [VBG*13].

Continuity: The positions of detail points continuously evolve with the parameters of sphere-mesh and there is no tearing of the surface. Indeed, a base-point can slide continuously along a bone and move from the conic part to the sphere part of the bone and conversely. Since the conic part is tangent to the sphere, both the base-point and its normal evolve continuously even in case of cone to sphere or sphere to cone base point motion. Since the heightfield of a detail-point is either preserved or continuously scaled, the whole motion is continuous throughout the deformation. Naturally, some base-points may become hidden because of a local intersection of the two bones of a joint being bent. We chose to keep these local intersections, since it will not degrade the resulting outer envelop of the model, which remains visually satisfying as if the surface became flattened in the fold of a joint [VBG*13]. Furthermore, if the base-point associated to a detail-point is hidden, the detail-point is also hidden in the fold of a joint. Figure 4 illustrates that our heightfield skinning can also be used for meshes by skinning the vertices heights, while keeping the connectivity fixed, at the risk of creating self-intersections or slivers, a risk shared by many mesh skinning methods (e.g. [TGB13]).

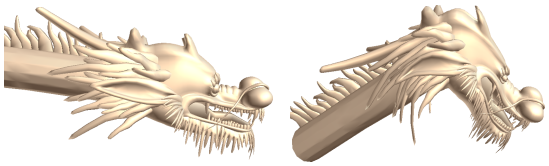

Figure 4: *Pose change for a mesh with folded surface sheets by heightfield skinning.*

Algorithm 1 Pose change using heightfield skinning

Input: Sphere-mesh model registered to the input point set P. Target pose and anatomy.
Output: Point set P' corresponding to the target changes.

1: Compute base point set $\tilde{P}$ corresponding to P on the registered sphere-mesh and compute the set of height values $h(P)$
2: Apply point set skinning on the base points $\tilde{P}$
3: Deform $\tilde{P}$ to the target pose and anatomy, yielding $\tilde{P}_{sk}$
4: Re-project points of $\tilde{P}_{sk}$ on the sphere-mesh yielding $\tilde{P}'$
5: Lift points $\tilde{P}'$ to the skin surface using the - possibly scaled - initial height of each point, yielding P'.

3.2.2. Base-point skinning

The skinning approach that we apply to the base-points is an alternative to classical skinning approaches [BP07, TGB13]. It could also have been used directly on the point-set details. Figure 5 compares the result of using a heightfield over base-point skinning with using directly point set skinning. Thus, in the following we describe the method in a generic point set context for notation simplicity.

The general idea of skinning is to attach each point to one or more bones with weights measuring the influence of each bone on

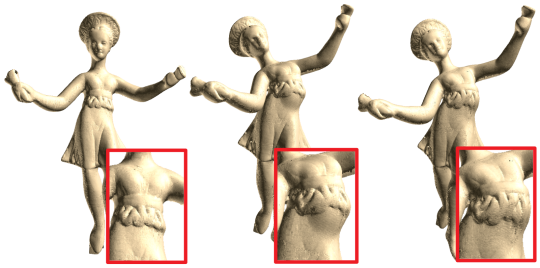

Figure 5: *Heightfield skinning. From left to right: original point set; pose change with direct point set skinning; pose change with heightfield skinning.*

it. The position of point after a deformation is a weighted linear combination of the positions relative to its influencing bones. Linear Blend Skinning [MTLT88], one of the most popular skinning method, causes some well-known collapsing problems at joints, in particular for large rotations. For example, the volume at joint is not preserved when it is bent around its axis (Figure 8a). Similarly, if we apply a twist around the axis of a bone while keeping its predecessor fixed, Linear Blend Skinning produces a folding of the joint around a singular point (Figure 9a). These flaws are avoided by Dual Quaternions Skinning [KCvO07] which interprets a combination of rigid transformations as a rigid transformation, however artefacts still appear in the concavities (Figure 8).

We propose to deal with the pose change in a different way that breaks down the movement into its natural components. Similar as [KSH12], we consider that the motion between two bones at a joint is the combination of a twisting rotation around the axis of one of the bones and a bending rotation around an axis perpendicular to both bones' axes. From there, we introduce motion-dependent skinning weights: the weight of a point is not the same for twisting and bending rotations. The impact of bending on the base point set should naturally be limited to an area loosely enclosing the rotating sphere joint, while the impact of twisting obviously extends to the length of the bones adjacent to the twisted articulation. This is more coherent with the fact that underlying muscles are arranged along the bones and attached to the joints. In our approach, a point $p \in P_k$ can only be influenced by the bones adjacent to B_k so that it has at least one and at most three weights.

Bending rotation with anisotropic weights. In order to overcome the artefacts that arise in the convex part of joints with Linear Blend Skinning, we use Dual Quaternions Skinning [KCvO07]. The weights of a point p during a bending rotation follow a Gaussian profile of the distances from p to each of the bones that influence it. It is driven by a parameter ε_r controlling the size of the influence area (Figure 6). In our experiments, we automatically set ε_r larger than the average distance between the point set and our model. If the skinning process is used on base-points on a sphere-mesh, we set ε_r value for a joint as a function of its radius and the length of the adjacent bones : $\varepsilon_r = 0.2 * \min(r_{k+1}, l_k - r_{k+1} - r_k, 0.5l_{k+1} - r_{k+1} - r_{k+2})$.

The weight $\omega_j(p)$, relative to one of p's influencing bones B_j writes:

$$\omega_j(p) = \frac{1}{c} \exp - \frac{\|p\tilde{p}_j\|^2}{2(\varepsilon_r/3)^2} \tag{3}$$

where c is a normalizing factor ensuring that the weights sum to 1, and $\tilde{p}_j$ is the orthogonal projection of p onto B_j, Hence if p is on bone B_j (as is the case for base-points), $\tilde{p}_j = p$. Figure 6 shows the weights profile along two bones.

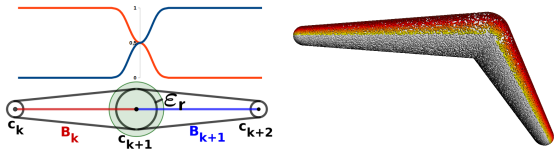

(a) **(b)**

Figure 6: *Skinning weights for the bending rotation around a joint. (a) the red curve represents the influence weights of the left bone B_k and the blue curve represents the influence of the right bone B_{k+1}. The influence area of each bone is controlled by ε_r. (b): values of anisotropic ε_r on a bone. Points such that $\varepsilon_r = 0$ are shown in white. From yellow to red, the value of ε_r increases linearly.*

However, it is possible to further improve the Dual Quaternions Skinning method, by noticing that if ε_r is large, the convex part behaves well with points sliding from the conic parts of both bones to the joint sphere, while an artefact is created in the concave part. On the contrary, if ε_r is close to 0, which corresponds to no skinning at all, a hole appears in the convex part, but a self-intersection is created in the concave part (Figure 7). Quite counter-intuitively, this self-intersection is much more visually satisfying than the thinning artefact observed otherwise. Indeed, only the outer envelop is visible and, when allowing self-intersection, this envelop is similar to the one obtained if a contact area was computed between the two bones [VBG*13]. To get the most of the two possibilities, we propose to adapt ε_r so that it is close to 0 for points in the concave part and it reaches its larger value for points on the convex parts. More precisely, ε_r varies continuously with respect to an *anisotropy angle* (See Figure 6).

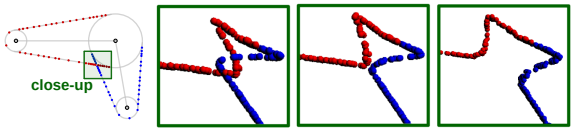

Figure 7: *Influence of ε_r on the skinning resulting from a bending rotation. In the first figure, $\varepsilon_r = 0$. The value ε_r increases from left to right.*

We define the anisotropy angle α_b at p as the angle between the plane defined by B_k and B_{k+1} axes and the plane defined by B_k's axis and p. This angle allows for a continuous transition over the skinned surface between points with no skinning, favoring local self-intersections ($\alpha_b \leq \pi/2$), and points with skinning, favoring the diffusion of points over the spherical joint surface ($\alpha_b \geq \pi/2$). Here, ε_r is deduced from the anisotropy angle as $\varepsilon_r = \cos\alpha_b \varepsilon'_r$, with

ε'_r controlling the influence area size. Therefore, the weight $\omega_j(p)$ associated to point p and one of its influencing bone B_j is:

$$\omega_j(p) = \begin{cases} \frac{1}{c} \quad \exp - \frac{\|p\tilde{p}_j\|^2}{2(\cos\alpha_b \frac{\varepsilon'_r}{3})^2} \text{ if } \cos\alpha_b < 0 \\ 1 \text{ if } \cos\alpha_b \geq 0 \text{ and } p \in P_j \\ 0 \text{ if } \cos\alpha_b \geq 0 \text{ and } p \notin P_j \end{cases} \quad (4)$$

(a) *Linear Blend skinning* **(b)** *Dual Quaternions skinning* **(c)** *Our anisotropic skinning*

Figure 8: *Comparison of our anisotropic skinning method with Linear Blend Skinning and Dual Quaternions for a bending rotation. For a fair comparison, the two first methods use the Gaussian weight of Equation 3 which is made anisotropic in our anisotropic skinning. Dual Quaternions fix the volume collapse of Linar Blend Skinning near the convexity, but artefacts remain in the concave part, while our skinning method does not suffer from any of these flaws.*

Twisting rotation. Let us consider a bone B_{k+1} twisted around its axis by an angle β, with its predecessor B_k kept fixed. Such a rotation impacts points attached to bones B_k and B_{k+1}. To handle this twist, we replace the linear combinations of bone motions with rotations adapted to the points. More precisely, each point is rotated around B_k's (resp. B_{k+1}) axis by an angle that depends on its distance to B_k (resp. B_{k+1}). For $p \in P_k$ rotating around the axis of B_k, this angle writes $\beta(p) = \omega(p)\beta$ with

$$\omega(p) = \frac{\|v_{k+1} - p^\star\|}{\|v_{k+1} - c_{k+1}\| + \|c_{k+1} - w_{k+1}\|} \quad (5)$$

$p^\star$ is the projection of p on B_k's axis, and v_{k+1} (resp. w_{k+1}) is a point on B_k's axis (resp. B_{k+1}) delimiting the impacted areas (Figure 10). By default $v_{k+1} = c_k$ and $w_{k+1} = c_{k+2}$, but different impacted areas can be designed by choosing different v_{k+1} and w_{k+1}. Here, the expression for $\omega(p)$ corresponds to a linear evolution of the rotation angle along the bone, but other types of influences could be designed. On Figures 9 and 10, we compare our method with Linear Blend Skinning and Dual Quaternions for a twisting rotation: the trace of the points initially aligned on a segment is much smoother with our approach.

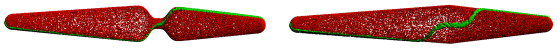

(a) *Linear Blend Skinning* **(b)** *Dual Quaternions Skinning*

Figure 9: *Twist motion: near blend Skinning and Dual Quaternions Skinning to be compared with our approach in figure 10 that uses twist specific weights. Green dots show points that were aligned before the twisting rotation.*

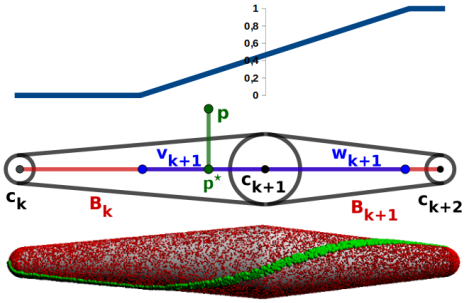

Figure 10: *The blue curve represents the value of ω_β. Points v_{k+1} and w_{k+1} define the range of the twisting effect of B_{k+1}. $p^\star$ is the projection of p on the skeleton line.*

Combination of twist and bend. Twist and bend specific skinning are combined to get the skinning result for any rotation around a joint. We perform first the twisting rotation and then the bending rotation. The positions and the weights of the points relative to each bone are updated between these two specific rotations.

3.3. Stage 3: Statue restoration by fragment combination

The last step of our virtual restoration process is to combine parts belonging to different statues after bringing them to a common pose and anatomy.

In the following, we note the registered model of the incomplete statue as $M_t = \{B_k(l_t^k, \mathbf{r}_t^k), \Theta_t^k\}_{k=1,..,22}$ and the registered model of the complementary statue, that is chosen to combine with the incomplete statue, as $M_c = \{B_k(l_c^k, \mathbf{r}_c^k), \Theta_c^k\}_{k=1,..,22}$. The size of a limb of missing parts is corrected by its existing symmetric limb after registration, if it exists. For example, we change the size of left arm of Wounded Amazon (Figure 14, fourth row) by the intrinsic parameters of its right arm. In case there is no clue for the size of a limb, such as for the missing arm, forearm and hand of the Esquiline Venus (Figure 14, first row), we use default human proportions. We change the overall elementary anatomy and pose of complementary model to match the incomplete statue using our heightfield skinning process. The pose for the missing parts is the same as the one in the complementary statue, unless some clue is given by some partial data. The position of one point p is computed by:

$$p = Skinning(Scale(\frac{l_t}{l_c}, \frac{\mathbf{r}_c}{\mathbf{r}_t}, \frac{\mathbf{r}_c}{\mathbf{r}_t})p)$$

where *Scale* is a scaling function to make the anatomy of the complementary statue correspond to the incomplete statue and *Skinning* is our heightfield skinning function. Re-scaling the complementary statue to adapt the incomplete statue is necessary for the reason that the morphology of two statues can be quite dissimilar. We show in Figure 11 a comparison of restoration results with and without morphology change. The leg we use to complete statue Spinario is too long and too large (See right image in Figure 11). After scaling the length and the radii with the parameters of the registered model, the restoration result is more satisfying.

At last, we integrate the selected parts into the incomplete statue.

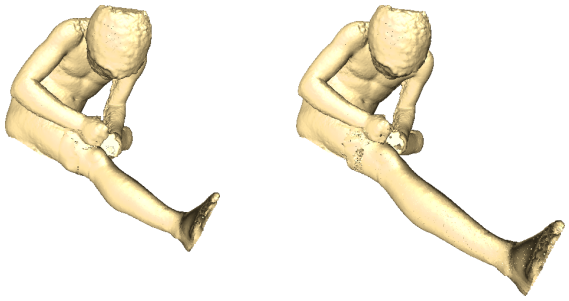

Figure 11: *The importance of morphology change in restoration. Left: restoration with scaling morphology of the leg part. Right: restoration using directly the original leg part.*

We assume that the selected parts and the statue to complete slightly overlap, which is necessary to blend harmoniously statue parts. In this overlap area, information must be merged.

Provided the details are not multi-layered above each sphere-mesh model in the overlap area, the part merging consists in removing the lower layer, creating a sharp boundary between the point sets, and then blending the points near the boundary. Recall that our sphere-mesh model is used as a basis surface to express the residual heightfield information h after the registration. We propose to use it to combine the data points. Let p be a point and $\tilde{p}$ its projection on the sphere-mesh model, we call Q_p be the subset of points of the two models that project on $\tilde{p}$, up to precision 3δ. The first step is to keep only the upper layer in the overlap area. To do so, we consider the subset H_p of the points in Q_p whose height values are larger than $h_{max} - \rho$, where h_{max} is the maximum height value for points in Q_p, and ρ is the average distance to the nearest neighbor for the points in the overlap area. Then we replace the height value of p by a Gaussian-weighted average of the height values in H_p. The resulting height value of p is thus:

$$h(p) = \frac{1}{S} \sum_{q \in H_p} e^{-\frac{\|\tilde{p}-\tilde{q}\|^2}{2(3\delta)^2}} h(q) \qquad (6)$$

with S a weight normalizing factor. This brings the points of the lower layer in the overlap area to the upper layer, creating a sharp boundary. Finally, the sharp boundary is smoothed by Gaussian-weighted averaging of the heightfield values across the boundary. The default value of *delta* is set to $3\delta = 10\rho$. A high value of *delta* smoothes the merging area but can cause distortions.

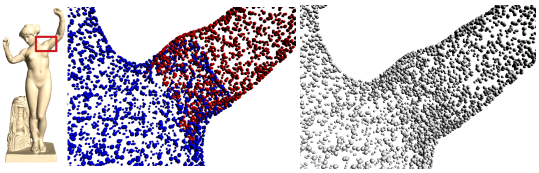

Figure 12: *Overlap area. Left: blue points and red points come from different statues. Right: Merging result.*

4. Results

In this section, we show the performance of our skinning method and results of virtual restoration. We developed our algorithm in C++, using OpenMP for computing point to bone distances in parallel. All experiments are run on an Intel Core i7-4790K CPU @ 4.00GHz.

We selected a set of statues from various sources. They are not all from the same archaeological period but the goal here is to illustrate the feasibility of our approach when one does not have a sufficiently rich set of data. Some of these models are incomplete and require restoration. Others are complete and can be used to complete or generate other statues.

Complete models:

1. Dancer with Crotales, Louvre Museum
2. Dancing Faun, Pompei excavations
3. Aphrodite, Thorvaldsens Museum
4. Saint John the Baptist, Ny Carlsberg Glyptotek

Incomplete models:

1. A plaster copy of Esquiline Venus, The Royal Cast Collection
2. A copy of The Old Fisherman, The Royal Cast Collection
3. A statue in the style of the Venus De Milo
4. Wounded amazon: Ny Carlsberg Glyptotek
5. Spinario: British Museum
6. Prince Paris, Ny Carlsberg Glyptotek

While the 'Dancer with crotales' is a raw point set. The other 9 models are point sets sampled on meshes extracted from the Sketchfab website.

Figure 13 shows the FAKIR registrations on four statues and compares resulting models after skeleton pose change and skinning with our method or skinning with Dual Quaternions. Our skinning method clearly improves the quality near bone joints. As can be seen in particular in the areas circled in red in the fourth column, our method suppresses or at least reduces the Dual Quaternions artefacts around the bone joints. Given a statue of 500000 points, FAKIR is performed on a subset of 10000 points, which takes about $5s$. Then the skinning process is applied to the whole set of points and takes less than $1s$, including computation of base points and re-projection.

In Figure 1, we show the process of completing a statue which lacks arms and legs. We can also change the pose of a statue after completion. For instance, we bring the Prince Paris statue to the pose of The Thinker statue. Indeed, sometimes the pose of a broken statue can not be deduced by its remain parts. In this case, we can give several hypotheses of its pose through our skinning algorithm.

Figure 14 shows the restoration of five other statues. The Esquiline Venus (first row) and the Venus de Milo (third row) are both missing arms while The Old Fisherman is missing legs (second row). The Wounded Amazon (fourth row) is missing an arm and the Spinario (fifth row) is missing a leg. The restoration method recovers plausible arms and legs in all five cases, leading to plausible restored statues. A limitation of our method is that sharp junction lines can be observed sometimes in the multi-layered area (See the Wounded Amazon in Figure 14). This due to the choice of δ in

equation 6. We make a compromise between a smooth fusion and a preservation of styles of both parts. The arms we have chosen for the two Venus statues are from masculine statues. Although the morphologies are quite different, our restoration merges the two parts in a satisfying manner. The legs we have chosen for The Old Fisherman have a different sculpture style, but again, our merging process blends in these two parts nicely. In our results, the choice of the complementary statues and the style of the restoration results may not correspond to the style of original statues. An art restorer with an expert knowledge of the statue history and artistic context would naturally better choose the complementary statues and control the restoration style.

5. Conclusion and perspectives

We introduced a framework for virtual restoration of human statues. For that purpose, we proposed a point set skinning method to modify the pose of the statue and applied it to virtual restoration by part combination. We compared our skinning approach with existing approaches to highlight its benefits. Thereafter, we will focus on solving the following problems. Sometimes, the point cloud from the scan of a statue is incomplete, or some areas, occluded in the original statue, are revealed by the pose change, creating thus a hole in the point set. In that case an inpainting process is necessary which we want to investigate in a future work. Finally, our current approach to combine parts remains basic and does not take the style into consideration. As a future work, we would like to design a combination approach more respectful of the style of the different fragments. In addition, we plan to develop a user-friendly interface so that users can simply choose candidate statues and compare different restoration hypotheses.

Acknowledgments This work was funded by the e-Roma project from the French Agence Nationale de la Recherche (ANR-16-CE38-0009). The *Dancer with crotales* model is a point set of the Farman Dataset [DAL*11]. The other 9 statues data are sampled on meshes from the Sketchfab website: the *Dancing Faun* model is courtesy of Moshe Caine, the *Venus de Milo* model is courtesy of Sketchfab user "tux", the *Spinario* model is courtesy of Sketchfab user "The British Museum" and the other 6 statues models (*Aphrodite*, *Saint John the Baptist*, *Esquiline Venus*, *Old Fisherman*, *Wounded Amazon* and *Prince Paris*) are courtesy of Geoffrey Marchal.

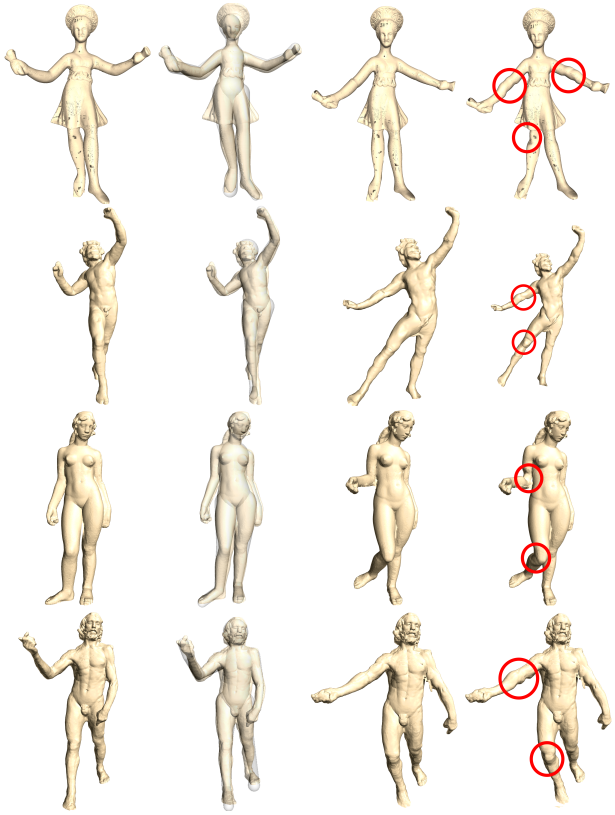

Figure 13: *Registration and pose changes of 4 statues: the Dancer with Crotales (first row), the Dancing Faun (second row), Aphrodite (third row) and the Old Man Walking (fourth row). First column: initial point set, second column: overlay of the registered model and the point cloud, third column: final point set in a modified pose by our skinning method, fourth column: skinning result with Dual Quaternions.*

References

[AL11] ARISTIDOU A., LASENBY J.: FABRIK: A fast, iterative solver for the inverse kinematics problem. *Graphical Models 73*, 5 (2011), 243–260. 2

[AMX*18] ALLDIECK T., MAGNOR M., XU W., THEOBALT C., PONS-MOLL G.: Video based reconstruction of 3d people models. In *CVPR* (2018), pp. 8387–8397. 2

[ARM*19] ANGLES B., REBAIN D., MACKLIN M., WYVILL B., BARTHE L., LEWIS J., VON DER PAHLEN J., IZADI S., VALENTIN J., BOUAZIZ S., ET AL.: Viper: Volume invariant position-based elastic rods. *Proceedings of the ACM on Computer Graphics and Interactive Techniques 2*, 2 (2019), 1–26. 2

[ASK*05] ANGUELOV D., SRINIVASAN P., KOLLER D., THRUN S., RODGERS J., DAVIS J.: Scape: shape completion and animation of people. *ACM TOG 24* (2005), 408–416. 2

[BKL*16] BOGO F., KANAZAWA A., LASSNER C., GEHLER P., ROMERO J., BLACK M. J.: Keep it SMPL: Automatic estimation of 3D human pose and shape from a single image. In *ECCV* (2016), pp. 561–578. 2

[BP07] BARAN I., POPOVIĆ J.: Automatic rigging and animation of 3d characters. *ACM TOG 26*, 3 (2007). 2, 4

[CK10] CHAUDHURI S., KOLTUN V.: Data-driven suggestions for creativity support in 3d modeling. *ACM TOG 29*, 6 (2010), 183:1–183:10. 2

[CKGK11] CHAUDHURI S., KALOGERAKIS E., GUIBAS L., KOLTUN V.: Probabilistic reasoning for assembly-based 3d modeling. *ACM TOG 30*, 4 (2011), 35:1–35:10. 2

[CSWS17] CAO Z., SIMON T., WEI S.-E., SHEIKH Y.: Realtime multi-person 2d pose estimation using part affinity fields. In *CVPR* (2017). 2

[DAL*11] DIGNE J., AUDFRAY N., LARTIGUE C., MEHDI-SOUZANI C., MOREL J.-M.: Farman Institute 3D Point Sets - High Precision 3D Data Sets. *IPOL* (2011). 8

[ED17] ELNAGHY H., DORST L.: Geometry based faceting of 3d digitized archaeological fragments. In *2017 IEEE International Conference on Computer Vision Workshops (ICCVW)* (2017), pp. 2934–2942. 1

[FCD20] FU T., CHAINE R., DIGNE J.: Fakir : An algorithm for estimat-

Figure 14: *Registration and restoration of 5 incomplete statues, Esquiline Venus (first row), Old Fisherman (second row), Venus de Milo (third row), Wounded Amazon (fourth row) and Spinario (fifth). First column: initial point set, second column: overlay of the registered model and the point set, third column: final restoration.*

ing the pose and elementary anatomy of archaeological statues. *to appear in Computer Graphics Forum, Proc. Pacific Graphics 2020* (2020). 2, 3

[FKS*04] FUNKHOUSER T., KAZHDAN M., SHILANE P., MIN P., KIEFER W., TAL A., RUSINKIEWICZ S., DOBKIN D.: Modeling by example. *ACM TOG 23*, 3 (2004), 652–663. 2

[GPT03] GROSSMAN J. B., PODANY J., TRUE M.: History of the restoration of ancient stone sculptures. 1

[HBL*17] HUANG Y., BOGO F., LASSNER C., KANAZAWA A., GEHLER P. V., ROMERO J., AKHTER I., BLACK M. J.: Towards accurate marker-less human shape and pose estimation over time. In *3DV* (2017). 2

[HFG*06] HUANG Q.-X., FLÖRY S., GELFAND N., HOFER M., POTTMANN H.: Reassembling fractured objects by geometric matching. *ACM TOG 25*, 3 (July 2006), 569–578. 1

[HLRB12] HIRSHBERG D. A., LOPER M., RACHLIN E., BLACK M. J.: Coregistration: Simultaneous alignment and modeling of articulated 3d shape. In *ECCV* (2012), pp. 242–255. 2

[HSS*09] HASLER N., STOLL C., SUNKEL M., ROSENHAHN B., SEIDEL H.-P.: A statistical model of human pose and body shape. *Computer Graphics Forum 28* (2009). 2

[Hus55] HUS A.: Sculpture étrusque archaïque : le cavalier marin de la villa giulia. *Mélanges de l'école française de Rome 67*, 1 (1955), 69–126. 3

[ICO64] ICOMOS: International charter for the conservation and restoration of monuments and sites. In *IInd International Congress of Architects and Technicians of Historic Monuments, Venice* (1964), pp. 25–31. 1

[JCZ19] JIANG H., CAI J., ZHENG J.: Skeleton-aware 3d human shape reconstruction from point clouds. In *ICCV* (2019), pp. 5431–5441. 2

[KCKK12] KALOGERAKIS E., CHAUDHURI S., KOLLER D., KOLTUN V.: A probabilistic model for component-based shape synthesis. *ACM TOG 31*, 4 (2012), 55:1–55:11. 2

[KCvO07] KAVAN L., COLLINS S., ŽÁRA J., O'SULLIVAN C.: Skinning with dual quaternions. In *I3D* (2007), ACM, pp. 39–46. 2, 5

[KSH12] KAVAN L., SORKINE-HORNUNG O.: Elasticity-inspired deformers for character articulation. *ACM TOG 31* (2012), 196:1–196:8. 2, 5

[Kv05] KAVAN L., ŽÁRA J.: Spherical blend skinning: A real-time deformation of articulated models. In *I3D* (2005), ACM, pp. 9–16. 2

[LCF00] LEWIS J. P., CORDNER M., FONG N.: Pose space deformation: A unified approach to shape interpolation and skeleton-driven deformation. In *ACM SIGGRAPH* (2000), pp. 165–172. 2

[LL19] LE B. H., LEWIS J. P.: Direct delta mush skinning and variants. *ACM TOG 38*, 4 (2019), 113:1–113:13. 2

[LMR*15] LOPER M., MAHMOOD N., ROMERO J., PONS-MOLL G., BLACK M. J.: SMPL: A skinned multi-person linear model. *ACM TOG 34*, 6 (2015), 248:1–248:16. 2

[LSS*19] LI C.-L., SIMON T., SARAGIH J., PÓCZOS B., SHEIKH Y.: Lbs autoencoder: Self-supervised fitting of articulated meshes to point clouds. In *CVPR* (2019), pp. 11967–11976. 2

[MMRC20] MARIN R., MELZI S., RODOLÀ E., CASTELLANI U.: Farm: Functional automatic registration method for 3d human bodies. *Computer Graphics Forum 39*, 1 (2020), 160–173. 2

[MTG03] MOHR A., TOKHEIM L., GLEICHER M.: Direct manipulation of interactive character skins. In *I3D* (2003), ACM, pp. 27–30. 2

[MTLT88] MAGNENAT-THALMANN N., LAPERRIÈRE R., THALMANN D.: Joint-dependent local deformations for hand animation and object grasping. In *Proceedings on Graphics Interface* (1988), Canadian Information Processing Society, pp. 26–33. 2, 5

[New34] NEWELL A. N.: Gallo-roman religious sculpture. *Greece and Rome 3*, 8 (1934), 74–84. 3

[PIT*16] PISHCHULIN L., INSAFUTDINOV E., TANG S., ANDRES B., ANDRILUKA M., GEHLER P., SCHIELE B.: Deepcut: Joint subset partition and labeling for multi person pose estimation. In *CVPR* (2016). 2

[PMG*05] PAULY M., MITRA N. J., GIESEN J., GROSS M., GUIBAS L. J.: Example-based 3d scan completion. In *SGP* (2005). 2

[PMRMB15] PONS-MOLL G., ROMERO J., MAHMOOD N., BLACK M. J.: Dyna: A model of dynamic human shape in motion. *ACM TOG 34*, 4 (2015), 120:1–120:14. 2

[POC05] POLICARPO F., OLIVEIRA M. M., COMBA J. A. L. D.: Real-time relief mapping on arbitrary polygonal surfaces. In *I3D* (2005), ACM, p. 155–162. 4

[SBB10] SIGAL L., BALAN A., BLACK M. J.: HumanEva: Synchronized video and motion capture dataset and baseline algorithm for evaluation of articulated human motion. *IJCV 87*, 1 (2010), 4–27. 2

[SHG*11] STOLL C., HASLER N., GALL J., SEIDEL H.-P., THEOBALT C.: Fast articulated motion tracking using a sums of gaussians body model. pp. 951–958. 2

[TGB13] THIERY J.-M., GUY E., BOUBEKEUR T.: Sphere-meshes: Shape approximation using spherical quadric error metrics. *ACM TOG 32*, 6 (2013). 2, 4

[VBG*13] VAILLANT R., BARTHE L., GUENNEBAUD G., CANI M.-P., ROHMER D., WYVILL B., GOURMEL O., PAULIN M.: Implicit skinning: real-time skin deformation with contact modeling. *ACM TOG 32*, 4 (2013), 125:1–125:12. 2, 4, 5

[WC91] WANG L.-C. T., CHEN C.-C.: A combined optimization method for solving the inverse kinematics problems of mechanical manipulators. *IEEE Transactions on Robotics and Automation 7* (1991), 489–499. 2

[WHB11] WEISS A., HIRSHBERG D., BLACK M. J.: Home 3d body scans from noisy image and range data. In *ICCV* (2011), pp. 1951–1958. 2

[WP02] WANG X. C., PHILLIPS C.: Multi-weight enveloping: Least-squares approximation techniques for skin animation. In *SCA* (2002), pp. 129–138. 2

[WZC12] WEI X., ZHANG P., CHAI J.: Accurate realtime full-body motion capture using a single depth camera. *ACM TOG 31* (2012). 2

[ZB15] ZUFFI S., BLACK M. J.: The stitched puppet: A graphical model of 3D human shape and pose. In *CVPR* (2015), pp. 3537–3546. 2